Springer

Journal of Mechanical Science and Technology 23 (2009) 2434~2443

Journal of Mechanical Science and Technology

www.springerlink.com/content/1738-494x
DOI 10.1007/s12206-009-0621-z

Simulation of droplet impact on a solid surface using the level contour reconstruction method †

Seungwon Shin[1,*] and Damir Juric[2]

[1]*Department of Mechanical and System Design Engineering, Hongik University, Seoul, 127-791, Korea*
[2]*Laboratoire d'Informatique pour la Mécanique et les Sciences de l'Ingénieur (LIMSI), CNRS-UPR 3251, 91403, Orsay, France*

(Manuscript Received November 20, 2008; Revised April 15, 2009; Accepted April 15, 2009)

Abstract

We simulate the three-dimensional impact of a droplet onto a solid surface using the level contour reconstruction method (LCRM). A Navier-slip dynamic contact line model is implemented in this method and contact angle hysteresis is accounted for by fixing the contact angle limits to prescribed advancing or receding angles. Computation of a distance function directly from the tracked interface enables a straightforward implementation of the contact line dynamic model in the LCRM. More general and sophisticated contact line models are readily applicable in this front tracking approach with few modifications, since complete knowledge of the geometrical information of the interface in the vicinity of the wall contact region is available. Several validation tests are performed including 2D planar droplet, 2D axisymmetric droplet, and full three-dimensional droplet splashing problems. The results show good agreement compared with existing numerical and experimental solutions.

Keywords: Contact line dynamics; Droplet impact; Front tracking; Multiphase flow; Numerical simulation; Surface tension

1. Introduction

Numerical treatment of the interface contact line at a solid wall bears great importance in helping to identify the underlying physics related to many engineering applications involving droplet splashing and nucleate boiling to name a few. The presence of a contact line further complicates the challenging task of multiphase flow simulation. In addition to the geometrical curvature and possible phase transformation effects at the interface, correct boundary conditions must be enforced near the wall contact region. A complete mathematical representation of the motion of an interface between immiscible fluids along a smooth solid surface is still a formidable task and several attempts have been made to provide macroscopic models of the contact line dynamics based on the microscopic physics.

Renardy et al. [1] implement a moving contact model in their volume-of-fluid (VOF) scheme with piecewise linear interface reconstruction. They treated the contact angle condition either by extrapolating the VOF function beyond the flow domain keeping its gradient perpendicular to the interface or by treating the problem as a three-phase situation mimicking the classical Young-Laplace equation. They devised a special convection scheme near the contact region to preserve mass. They found that the extrapolation method with interface slip is preferable to the three-phase approach.

A more complex three-dimensional case of droplet splashing onto an asymmetric surface using an Eulerian fixed-grid algorithm with a volume tracking approach has been treated by Bussman et al. [2]. Contact angles are applied as a boundary condition at the contact line. They performed simulations of oblique impact of a droplet onto a wall and compared this to experimental results. Photographic results showed

† This paper was recommended for publication in revised form by Associate Editor Gihun Son

*Corresponding author. Tel.: +82 2 320 3038, Fax.: +82 2 3227003
E-mail address: sshin@hongik.ac.kr

very good agreement with numerical simulations which use contact angle information evaluated from the experiment for boundary conditions. They also tested a simpler model which imposes the contact angle as a function of the contact line speed and found similar results.

Sikalo et al. [3] used the VOF based free surface capturing method to compare their experimental results for a droplet impacting a solid wall. The drop spreading diameter and dynamic contact angle are measured and compared with numerical solution. They used a local body force with some dependence on contact line speed in determining the dynamic contact angle. They obtained good agreement between experiment and numerical simulation. They also found that the dynamic contact angle is a function of the flow field in the vicinity of the moving contact line as well as contact line speed. Therefore, a unique functional dependence of dynamic contact angle to contact angle speed was difficult to obtain. The static contact angle has a minimal effect on the dynamic contact angle over a wide range of experimental data during the spreading stage.

Gunjal et al. [4] simulated the process of sequential spreading and recoil of a liquid droplet over a long period of time after collision with a flat solid surface using the VOF method. The experimental results are compared to CFD simulations. Numerical results showed reasonably good agreement compared to the experiment. The contact line can move along the wall by modifying the surface normal using the tangential/normal vector and contact angle at the wall. Despite the no-slip boundary condition at the solid wall, wall movement was natural for their simulation since the non-zero fluid velocities adjacent to the wall influenced the movement of the contact line point.

Fukai et al. [6] upgraded their previous method [5] to include effects of inertia, viscosity, gravitation, surface tension forces, and contact angle hysteresis. Their model is based on the finite element technique accompanied by a Lagrangian approach to account for accurate simulation of the interface deformation. Precise interfacial boundary conditions can be applied directly onto the surface and the value of the dynamic contact angle depends on the contact line velocity. They presented both experimental and computational results for a water droplet impacting the wall under various conditions. The experimentally determined contact angle was used in the numerical simulation. Droplet deformation, splat radius, and splat height from the numerical solution were compared with experiment and good agreement was obtained not only in the early spreading phase but also during the recoil and oscillation phase. They also found that the wettability model is more crucial, not during the early stage inertia dominated region but rather after the initiation of the recoil process.

Spelt [7] extended the level set method (LSM) to simulate multiple contact lines while accounting for the effects of inertia, contact-line hysteresis, and slip. Grid convergence tests were performed and solutions were compared to other existing theories. To alleviate the stress singularity at the contact region, they prescribed either the contact line speed or the contact angles at the wall during the simulation. In both cases, the interface must be permitted to slip along the wall, and the slip condition associated with the contact angle or contact line speed was applied to the entire wall. A converged solution with increased resolution was obtained for the interfacial shape and stress along the wall. Reasonable agreement is obtained between simulation and analytic results from the lubrication theory.

Liu et al. [8] also developed a contact line model in the context of a sharp interface Cartesian grid level set method. They applied the Navier-slip boundary condition in the vicinity of the contact lines, which allows interface slip in the direction tangential to the substrate, thus avoiding a stress singularity. The slip condition is only applied to the fluid points near the contact lines and the grid spacing was chosen for the slip distance. They recalculated the local level set function field to set the distance function correctly near the contact points. The distance function was reinitialized to give the correct contact angle through the wall. They compared their results with those of Fukai et al. [6] and obtained good agreement. The maximum spread radius and droplet thickness was underestimated, but the spread radius showed excellent agreement after the peak value. They also tested a water droplet impacting on an arbitrary surface such as inclined, curved, and cylindrical surfaces. The results provided qualitatively correct solutions.

The above-mentioned approaches have found success but have been limited to front capturing type methods where the phase interface is captured or in some way defined on a fixed grid and mostly to two-dimensional simulations of multiphase flow problems. Accurate modeling of contact line dynamics poses additional numerical challenges for three-dimensional

interface simulations especially for front tracking type methods due to the difficulty of assigning correct boundary condition where the interface cross the domain boundaries as well as bookkeeping of logical connectivity between interface elements. We have developed the level contour reconstruction method (LCRM), which combines the characteristics of level set and front tracking methods [9-12]. Recently, we added a new procedure for calculating the distance function field directly from the interface for the level contour reconstruction method [9]. This alleviates the problem of defining a continuous boundary condition where the interface touches the wall. The front tracking based LCRM also enables us to locate contact points (2D) or lines (3D) precisely on the wall along with the contact angle.

In this paper, we will present a procedure for the treatment of the wall contact problem in the level contour reconstruction method. Focus has been placed on three-dimensional simulations since the LCRM was originally designed and optimized for 3D problems.

2. Numerical formulation

2.1 Governing equations

The following single field formulation of the continuity and momentum equations is solved for incompressible multiphase flow:

$$\nabla \cdot \mathbf{u} = 0 \tag{1}$$

$$\rho\left(\frac{\partial \mathbf{u}}{\partial t} + \mathbf{u} \cdot \nabla \mathbf{u}\right) = -\nabla P + \rho \mathbf{g} + \nabla \cdot \mu(\nabla \mathbf{u} + \nabla \mathbf{u}^{\mathrm{T}}) + \mathbf{F} \tag{2}$$

where $\mathbf{u}$ is the velocity vector, P the pressure and $\boldsymbol{g}$ the gravitational acceleration.

Material property fields can be described by using the indicator function, $I(\mathbf{x},t)$, a Heaviside function which varies from zero to one near the interface. For example, the density is calculated by:

$$\rho(\mathbf{x},t) = \rho_1 + (\rho_2 - \rho_1) I(\mathbf{x},t) \tag{3}$$

where the subscripts 1 and 2 refer to the respective fluids. A similar equation is used to define the viscosity, μ. The interface is advected in a Lagrangian fashion by integrating

$$\frac{\mathrm{d}\mathbf{x}_f}{\mathrm{d}t} = \mathbf{V} \tag{4}$$

where $\mathbf{V}$ is the interface velocity vector interpolated at $\mathbf{x}_f$.

The hybrid formulation [11] with compact curvature support [9] is used for the local surface tension force at the interface, $\mathbf{F}$. Interface evolution is tracked using the level contour reconstruction method with a high order reconstruction procedure [12]. The detailed numerical process for solving the above governing equations can be found in [9-12]. Here we focus on numerical treatment of the boundary conditions with wall contact of the interface.

2.2 Treatment of indicator function near the contact line

In the original front tracking method, the Indicator function, I, can be found by solving the following Poisson equation with a standard FFT package such as FISHPAK [13] on a uniform Cartesian grid:

$$\nabla^2 I = \nabla \cdot \int_{\Gamma(t)} \mathbf{n}_f \delta_f(\mathbf{x} - \mathbf{x}_f)\mathrm{d}s \tag{5}$$

where $\mathbf{n}_f$ is the unit normal to the interface, $\mathbf{x}_f = \mathbf{x}(s,t)$ is a parameterization of the interface $\Gamma(t)$, and $\delta_f(\mathbf{x}\text{-}\mathbf{x}_f)$ is a three-dimensional Dirac distribution that is non-zero only when $\mathbf{x} = \mathbf{x}_f$. ds is the length (2D) or area (3D) of the element.

Without interface contact or domain boundary crossing, it is obvious that we can assign the boundary values of I with explicit Dirichlet conditions, i.e., values of one or zero. In the case of the interface touching the simulation domain boundary, it becomes complicated to implement correct boundary conditions. Khenner [14] developed a simple and robust procedure for accurate computation of indicator function values where the interface crosses the simulation boundary for the front tracking method. However, to calculate the correct transition of the indicator function through the boundary, a few iterations were generally required.

An indicator function field which has the characteristics of a Heaviside function can also be found by using the distance function as in the level set method. Based on the idea that the level contour reconstruction method has characteristics of the level set method,

we have developed a new procedure for computing a vector distance function from the existing interface and reconstructing the interface using the resulting distance function field [9]. Here, we will describe the basic idea briefly. For a given interfacial element, we can identify a sufficiently large local neighborhood of grid nodes and calculate the minimum distance to that element and where on that element the minimum distance point lies as can be seen from Fig. 1. The correct sign function can be easily identified for each grid node since the interface element already has a specific orientation given by its normal which is pointing toward phase 2 as shown in Fig. 1. This minimum distance vector can originate either from a point inside the line segment of the element (point B_{bt} in Fig. 1) or from the edge of the element (point A_{bt} in Fig. 1). After sweeping through all of the elements, we can construct the final distance function value at each grid node as well as the minimal distance point on the interface element. In this way, the distance function field can be calculated for cells neighboring the interface, usually 6 cells wide in each direction (gray area in Fig. 1), and, to save resources, we can denote the distance function away from this strip as an arbitrary sufficiently large number. The complete procedure for 2D and 3D implementation can be found in [9].

The indicator function field calculated from the above procedure near the contact line has been shown in Fig. 2. We observed a smooth transition of the indicator function across the interface and correct representation of the advancing contact angle which has been prescribed as 120^o.

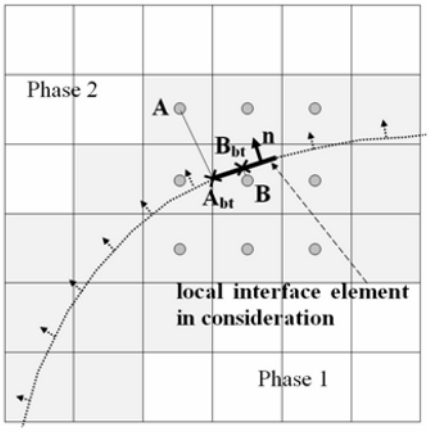

Fig. 1. Schematic diagram for computing distance function for 2D simulation.

2.3 Contact line dynamic modeling

Numerical implementation of a complete mathematical formulation which accounts for complex interfacial physics associated with microlayer effects near the contact line is still a formidable task and the exact nature of the contact line motion still remains poorly understood. We are usually interested in the macroscopic behavior of interfacial deformation near a solid surface and simplified models have been successfully used in many cases in the literature [1-8]. Therefore, we will confine our work to macroscopic modeling of contact line dynamics.

With a no-slip boundary condition at the wall, the shear stress becomes infinite near the contact line. To alleviate this infinite shear stress, various numerical techniques have been developed [1-8, 14]. One approach is to use the Navier-slip model [8], which allows contact line movement proportional to shear stress at the contact point. We use the Navier-slip model here to account for the contact line behavior at the boundary wall. The contact line velocity can be determined by the following equation:

$$U_{cl} = \lambda \left. \frac{\partial u}{\partial n} \right|_{wall} \tag{6}$$

here, U_{cl} denotes the contact line speed, $\partial u/\partial n\,|_{wall}$ is the shear strain rate at the wall, and λ is a proportionality constant. In most cases, we choose λ to be the size of a grid cell as proposed by Liu *et al*. [8].

Since we have explicit information on the interface, it is relatively straightforward to implement contact line dynamics in the current method. Fig. 3 illustrates the procedure for implementing the contact line model in the LCRM. First, we identify the "contact point" (or contact line in 3D). The interface element containing this contact point will form a near wall layer. By

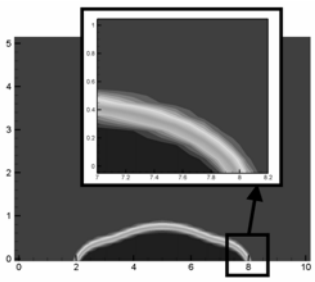

Fig. 2. Indicator function field calculated near the the contact point in 2D simulation.

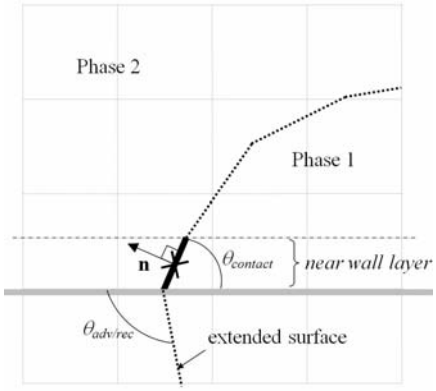

Fig. 3. Schematic diagram of contact line dynamic modeling in LCRM.

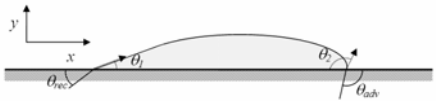

Fig. 4. Example of the contact angle model implementation in 2D simulation.

calculating the interface normal for the near wall interfaces, we can identify the contact angles associated with those contact points. We then extend the interface outside the wall to correctly impose the interfacial source term in the governing equations. The model should also account for contact angle hysteresis and static contact angle. Generally, the relation between contact line speed and contact angle has been poorly understood. Therefore, a very simple hysteresis model has been applied as follows:

$$\begin{cases} \theta = \theta_{adv} & if \quad \theta > \theta_{adv} \\ \theta = \theta_{rec} & if \quad \theta < \theta_{rec} \\ \theta_{adv} < \theta < \theta_{rec} & otherwise \end{cases} \tag{7}$$

We assumed constant advancing (θ_{adv}) and receding (θ_{rec}) contact angles. If the current contact angle, θ, is less than the prescribed receding angle (θ_{rec}) or greater than the advancing angle (θ_{adv}), then the interface will be extended with the given receding or advancing contact angle, respectively. If the contact angle is between the advancing and receding angles, we use the current contact angle without modification. Fig. 4 shows a typical case for the contact angle model implementation in a two-dimensional simulation. θ_2 is greater than the advancing contact angle; thus the interface is extended with the advancing contact angle, θ_{adv}. The receding contact angle, θ_{rec} , is used to extend the interface at the contact point with contact angle of θ_1 which has a smaller value than the receding contact angle. During hysteresis, no fixed contact angle is imposed and the contact angle is free to move between the advancing and receding angles. A more sophisticated contact model such as one with a linear dependence of the contact angle on contact line speed could be readily applied with few modifications if such a relation were supplied.

3. Results and discussion

3.1 Convergence tests

We considered a droplet splashing problem in planar geometry. The dimensionless groups resulting from non-dimensionalization of the governing equations are the Reynolds, Weber, and Bond number defined as follows:

$$\mathrm{Re} = \frac{\rho U_o R}{\mu}, \mathrm{We} = \frac{\rho U_o{}^2 R}{\sigma}, \mathrm{Bo} = \frac{\rho g R^2}{\sigma} \tag{8}$$

where ρ is liquid density, μ is liquid viscosity, σ is the surface tension coefficient, U_o is the impact velocity, R is droplet radius, and g is gravitational acceleration. Initially a circular droplet with non-dimensional radius of 1.0 is placed right above the wall within a 10×5 domain. The droplet impacts the wall with unit non-dimensional impact velocity. A Reynolds number of 100, Weber number of 10, and Bond number of 0.5 are used for the simulation. The gas/liquid density and viscosity ratios are 0.01 and 0.1, respectively. For this problem, an advancing angle of 92^o and receding angle of 60^o have been chosen as the prescribed contact angles. No-slip velocity conditions are applied to the four walls.

We first tested convergence of the simulation as we increased grid resolution. Fig. 5 shows both the maximum height of the droplet and one-half of the contact length during the simulation. The contact length can be calculated by detecting the maximum and minimum x location of contact points at the wall. As can be seen from the figure, the solution converges with increasing grid resolution. Fig. 6 shows volume conservation relative to grid resolution. Total mass loss is 7.8% for 50×25 grid resolution, 3.4% for 100×50, 0.74% for 200×100, and 0.35% for 400×200. Volume

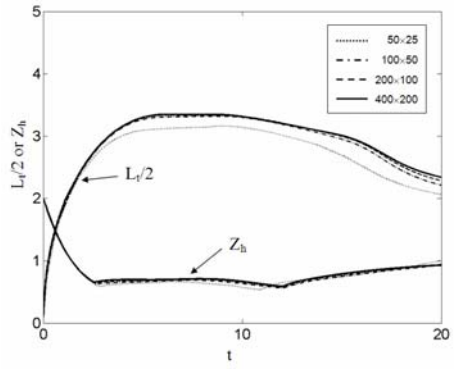

Fig. 5. Maximum height of the droplet and one-half of the contact length.vs time for 2D planar droplet splashing simulation.

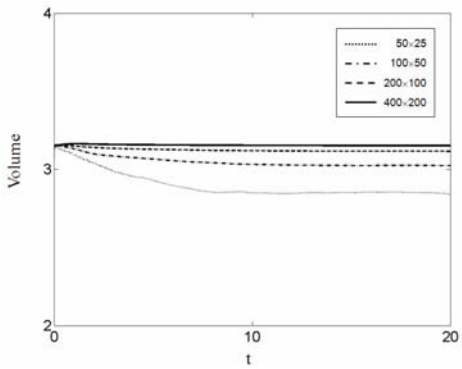

Fig. 6. Mass conservation during 2D planar droplet splashing simulation.

conservation converges with increasing resolution and mass loss is not significant with sufficient resolution.

3.2 2D axisymmetric droplet splashing

To compare with realistic situations, we used the same conditions described by Fukai *et al*. [6], where Re = 3130, We = 64.1, Bo = 0.468. Here we used an advancing angle of 92^o and receding angle of 60^o with 256×256 grid resolution for a 5×5 domain. A no-slip boundary condition at the bottom wall and symmetric boundary condition at r = 0 is applied. We used open conditions at r = 5 and the top wall. A droplet with unit impact velocity is placed right above the bottom wall with unit initial radius. The sequence of deformation of the droplet is shown in Fig. 8. For a clear comparison, the plot times have been chosen to the corresponding times presented by Fukai *et al*. [6]. As can be seen from the figure, a thin film is formed

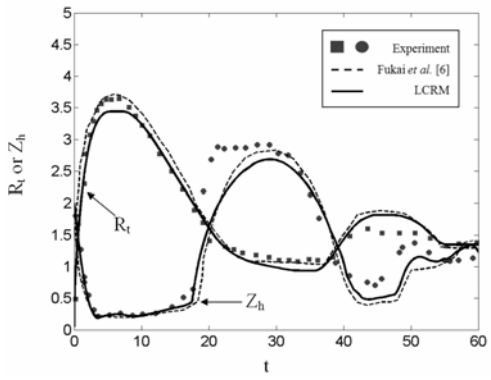

Fig. 7. Sequential deformation plots of the 2D axisymmetric droplet interface.

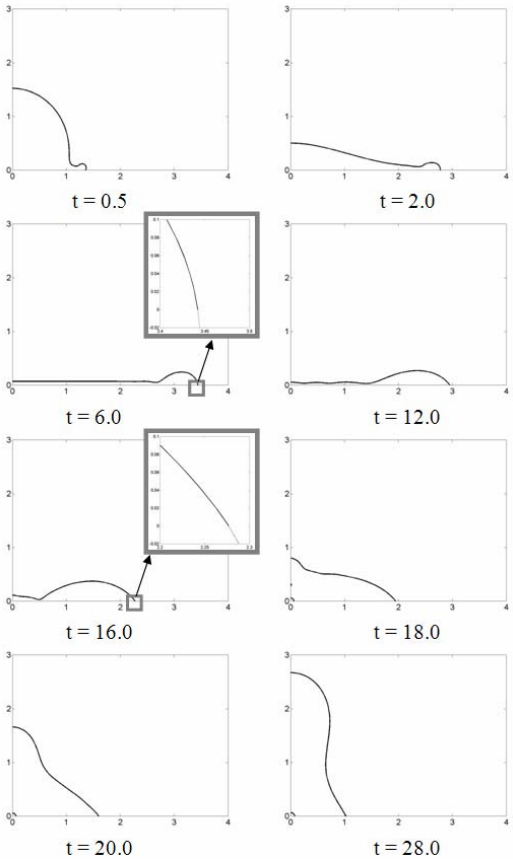

Fig. 8. Comparison of the current simulation result with both simulation and experimental results by Fukai *et al.* [6].

right after impact and rolls back after approximately t = 7. In the magnified window at t = 6.0 in Fig. 8, we plotted the extended interface at the contact region. We can clearly see that the contact angle maintains its advancing value of 92^o for spreading. The flow re-

verses at approximately $t = 10$, and we again can see that the interface has the correct receding angle of 60° during this recoil process (magnified window at $t = 16.0$ in Fig. 8). The droplet center rebounds up near $t = 18.0$ and keeps oscillating until equilibrium.

Fig. 7 shows a comparison of the current result with both a simulation by Fukai *et al.* [6] and their experimental results. Overall, the current simulation shows a close match compared to the simulation results obtained by Fukai *et al*. [6]. The maximum spread radius which occurs around $t = 8.0$ was 3.44 for the current simulation, which is somewhat smaller than the experimental value of 3.6. The maximum droplet thickness at time near 30.0 for the current simulation is 2.67, which is slightly different from the simulation result of 2.8 by Fukai *et al*. [6]. Total mass loss during the entire simulation period was 1.5 %. The deviation of splat radius as well as maximum droplet thickness from experimental results could be attributed to the limitations of the axisymmetric simulation geometry. However we have also used contact angle hysteresis with simply prescribed constant advancing and receding angles which may not match the experimental conditions. Complete three-dimensional simulations with more sophisticated contact line modeling, which allows linear variation of advancing and receding contact angles associated with the shear stress at contact points, will likely show more physically appealing results and is currently under investigation.

3.3 3D droplet impact on a slanted wall

To compare our model under fully three dimensional conditions, we present simulation results corresponding to those of Bussmann *et al.* [2]. A droplet with diameter of 2 mm is placed right above a wall inclined at 45°. Pre-impact velocity is 1 m/s and properties of water and air at atmospheric pressure have been chosen for droplet and ambient gas, respectively. For contact angle hysteresis, an advancing angle of 110° and receding angle of 40° have been chosen for the simulation. We simulated the full domain of 8 mm × 6 mm × 3 mm with 120×90×45 grid resolution in each x, y, and z direction, respectively. This resolution corresponds to 15 cpr (cells per radius) in Bussman *et al.* [2]. Open conditions have been applied at all boundary faces except the bottom wall where $z = 0$. Initial impact occurs near the y-z plane with $x = 0$.

The results for interface shape from our simulation (corresponding to the results of Bussmann *et al.* [2]) are shown in Fig. 9. The left side of Fig. 9 is a side view of the interface evolution and the right side is a top view. Although the results of Bussmann *et al.* [2] are not reproduced here, the interface shape is very close to the result they obtained. In Fig. 10, we present the actual triangular interface elements at $t = 3$ ms with the extended surface at the region of the contact line. We can clearly see that the advancing angle of 110° and receding angle of 40° have been maintained correctly during interfacial development. The spread factor measured as the difference between the location of the leading edge and trailing edge scaled by the diameter shows good quantitative agreement compared to the experimental and numerical results of Bussman *et al.* [2] (Fig. 11). The maximum spread factor becomes nearly constant near the later stage of impact for current simulation, a feature which has not been captured by Bussman *et al.* [2].

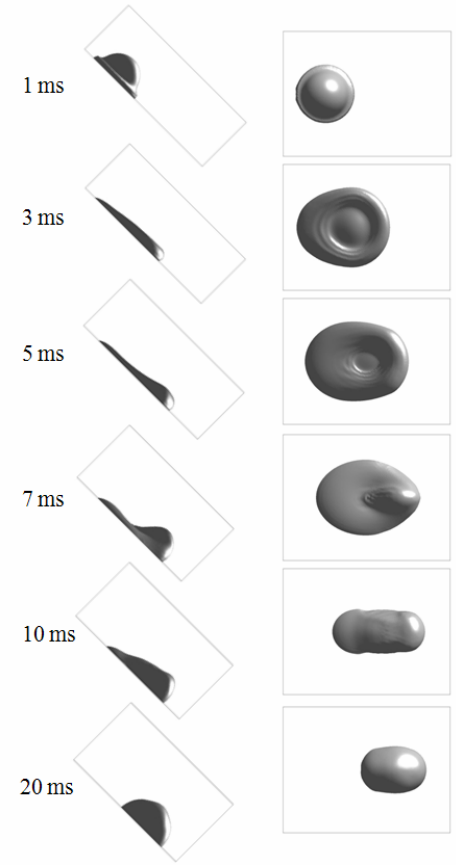

Fig. 9. Interface plots for 3D droplet impact on the slanted wall.

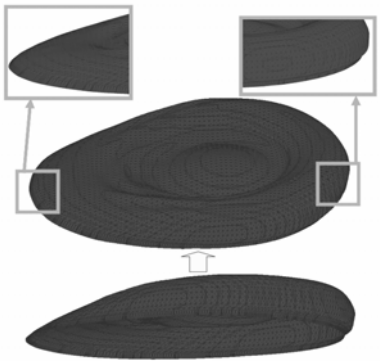

Fig. 10. Interface plot at t = 3 ms with the extended surface at the region of the contact line.

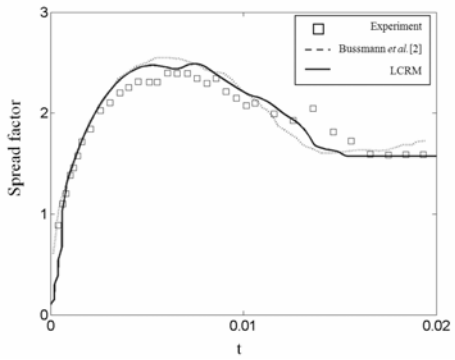

Fig. 11. Comparison of spread factor with experimental results from Bussman *et al.* [2].

3.4 3D multiple droplet impact

As a final test for more complex evolution of the interface along with contact dynamics, we simulated the impact of multiple droplets in a rectangular geometry. A domain size of 8 mm × 8 mm × 4 mm with a 60×60×30 grid resolution has been used for the simulation. The same material properties and contact angle hysteresis as those of section 3.3 are used and the droplet radii range from 0.5 mm to 1.25 mm. Seven droplets are initially positioned at randomly chosen locations of (2.4, 4.4, 2), (2, 2, 0.65), (6, 2.4, 1), (5.6, 5.6, 3), (4, 1.6, 2), (2, 6.8, 1), and (4.4, 4, 1.2). All units are mm and the x, y, z coordinates have been provided sequentially. The radii of the droplets are 1 mm, 0.5 mm, 0.65 mm, 0.85 mm, 1.25 mm, 0.75 mm, and 0.7 mm, respectively. The droplets impact the wall with random velocity and direction of (0.1, 0.15, -0.25), (0.1, -0.1, -0.5), (0.1, 0.05, -0.1), (0.1, 0.1, -0.35), (0.0, 0.15, -0.3), (0.1, 0.0, -0.3), and (0.3, 0.45, -0.75). All units are m/s and each directional velocity

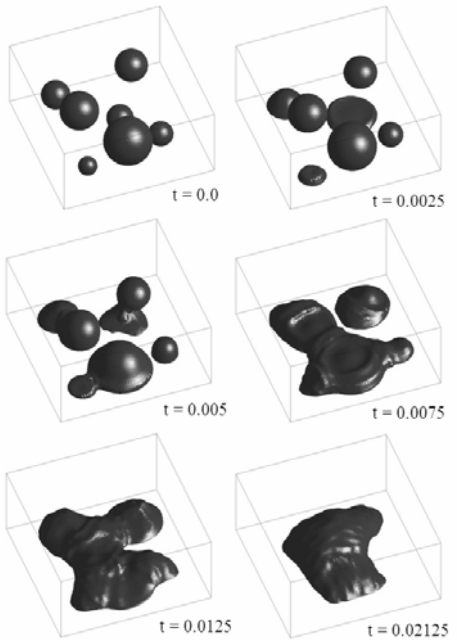

Fig. 12. Interface evolution plot for 3D multiple droplet impact.

u, v, w in space has been provided sequentially. Open boundary conditions are applied at all faces except no-slip at the bottom wall. As can be seen in Fig. 12, the phase interface experiences extremely dynamic deformation along with very complex contact line behavior. We can furthermore observe that the current model can capture the sophisticated nature of the contact line dynamics qualitatively along with interface merging and breakup. More quantitative research should be followed and is currently under investigation.

4. Conclusions

Even though the front tracking method, which explicitly tracks the evolution of the interface, can permit the precise location of contact points (2D) or lines (3D), multiphase modeling with contact line dynamics was relatively scarce for front tracking type simulation. This is partly due to the complexity of bookkeeping logical connectivity between interface elements, but mostly to assigning correct boundary conditions at domain boundaries with interface contact. We developed a new procedure for computing an indicator function field directly from the distance function, which in turn is generated directly from

knowledge of the interface location and orientation for the level contour reconstruction method. The resulting indicator function field is quite continuous and smooth without further modification of the procedure. Furthermore, the Level Contour Reconstruction Method, which has all the characteristics of front tracking, makes the implementation of a contact line model relatively straightforward.

Since a complete microscale formulation of contact line dynamics is still a subject of investigation, and since it is the apparent behavior of the interface contacting the wall that holds a great deal of interest, we have focused on macroscopic modeling of contact line dynamics. We used a simple Navier-slip condition as our contact line dynamic model and accounted for contact angle hysteresis by fixing the contact angle to the prescribed advancing or receding angles if the current contact angle is greater or less than the advancing or receding angles, respectively. We have tested a 2D droplet splash problem in planar geometry. The results showed good grid convergence and mass conservation. To compare with a more realistic situation, 2D axisymmetric droplet and fully three-dimensional splashing tests were performed, and data from these simulations compared well with existing numerical solutions and experimental data. We also observed that the current model can capture complex evolution of the interface motion along with contact dynamics. These, to our knowledge, are the first front-tracking type computations for the general 3D droplet impact problem.

Even though we have used a very simple contact line dynamic model, a more sophisticated contact model can be readily applied with minor modifications since, with a tracked interface, we have full knowledge of geometric quantities pertaining to the wall contact region.

Acknowledgment

This work was supported by the Korea Research Foundation Grant funded by the Korean Government (MOEHRD, Basic Research Promotion Fund) (KRF-2007-331-D00058) and by computer resources of the Institut du Développement et des Ressources en Informatique Scientifique (IDRIS) of the CNRS, France.

References

[1] M. Renardy, Y. Renardy and J. Liu, Numerical simulation of moving contact line problems using a volume-of-fluid method, *J. Comput. Phys*., 171 (2001) 243-263.

[2] M. Bussmann, J. Mostaghimi and S. Chandra, On a three-dimensional volume tracking model of droplet impact, *Phys. Fluids*, 11 (1999) 1406-1417.

[3] S. Sikalo, H. D. Wilhelm, I. V. Roisman, S. Jakirlic and C. Tropea, Dynamic contact angle of spreading droplets: experiments and simulations, *Phys. Fluids*, 17 (2005) 062103.

[4] P. R. Gunjal, V. V. Ranade and R. V. Chaudhari, Dynamics of drop impact on solid surface: experiments and VOF simulations, *AIChE Journal*, 51 (2005) 59-78.

[5] J. Fukai, Z. Zhao, D. Poulikakkos, C. M. Megaridis and O. Miyatake, Modeling of the deformation of a liquid droplet impinging upon a flat surface, *Phys. Fluids*, 5 (1993) 2588-2599.

[6] J. Fukai, Y. Shiiba, T. Yamamoto, O. Miyatake, D. Poulikakkos, C. M. Megaridis and Z. Zhao, Wetting effects on the spreading of a liquid droplet colliding with a flat surface: experiment and modeling, *Phys. Fluids*, 7 (1995) 236-247.

[7] P. D. M. Spelt, A level-set approach for simulations of flows with multiple moving contact lines with hysteresis, *J. Comput. Phys*., 207 (2005) 389-404.

[8] H. Liu, S. Krishnan, S. Marella and H. S. Udaykumar, Sharp interface Cartesian grid method II: a technique for simulating droplet interactions with surfaces of arbitrary shape, *J. Comput. Phys*., 210 (2005) 32-54.

[9] S. Shin and D. Juric, A hybrid interface method for three-dimensional multiphase flows based on front tracking and level set techniques, *Int. J. Num. Meth. Fluids* 60(7) (2009) 753-778.

[10] S. Shin and D. Juric, Modeling three-dimensional multiphase flow using a level contour reconstruction method for front tracking without connectivity, *J. Comput. Phys*., 180 (2002) 427-470.

[11] S. Shin, S. I. Abdel-Khalik, V. Daru and D. Juric, Accurate representaion of surface tension using the level contour reconstruction method, *J. Comput. Phys*., 203 (2005) 493-516.

[12] S. Shin and D. Juric, High order level contour reconstruction method, *Journal of Mechanical Science and Technology*, 21 (2007) 311-326.

[13] P. N. Swarztrauber and R. A. Sweet, Efficient Fortran Subprograms for the Solution of Separable Elliptic Partial Differential Equations, *ACM Transactions on Mathematical Software*, 5 (1979) 352-364.

[14] M. Khenner, Computation of the material indicator function near the contact line (in Tryggvason's method), *J. Comput. Phys*., 200 (2004) 1-7.

Seungwon Shin received his B.S. and M.S. degrees in Mechanical Engineering from Seoul National University, Korea, in 1995 and 1998, respectively. He then received his Ph.D. from Georgia Tech in 2002. Dr. Shin is currently a Professor at the School of Mechanical and System Design Engineering at Hongik University in Seoul, Korea. His research interests include computational fluid dynamics, multiphase flow, surface tension effect, phase change process.

Damir Juric received his B.S. and M.S. degrees in Mechanical Engineering from Worcester Polytechnic Institute in 1987 and 1990, respectively and his Ph.D. from the University of Michigan in 1996. Dr. Juric has worked in industry, academia and government and is currently Chargé de Recherche at the CNRS in Orsay, France. His research interests are in computational physics, fluid dynamics and interface methods for multiphase flow.